Electron irradiation reveals robust fully gapped superconductivity in $LaNiGa_2$

S. Ghimire,[1,2] K. R. Joshi,[1,2] E. H. Krenkel,[1,2] M. A. Tanatar,[1,2] Yunshu Shi,[3] M. Kończykowski,[4] R. Grasset,[4] V. Taufour,[3] P. P. Orth,[1,2,5] M. S. Scheurer,[6] and R. Prozorov[1,2,*]

[1]*Ames National Laboratory, Ames, Iowa 50011, USA*

[2]*Department of Physics & Astronomy, Iowa State University, Ames, Iowa 50011, USA*

[3]*Department of Physics and Astronomy, University of California, Davis, California 95616, USA*

[4]*Laboratoire des Solides Irradiés, CEA/DRF/IRAMIS, École Polytechnique, CNRS, Institut Polytechnique de Paris, F-91128 Palaiseau, France*

[5]*Department of Physics, Saarland University, 66123 Saarbrücken, Germany*

[6]*Institute for Theoretical Physics III, University of Stuttgart, 70550 Stuttgart, Germany*

(Received 14 November 2023; revised 24 December 2023; accepted 16 January 2024; published 29 January 2024)

The effects of 2.5-MeV electron irradiation were studied in the superconducting phase of single crystals of $LaNiGa_2$, using measurements of electrical transport and radio-frequency magnetic susceptibility. The London penetration depth is found to vary exponentially with temperature, suggesting a fully gapped Fermi surface. The inferred superfluid density is close to that of a single-gap weak-coupling isotropic *s*-wave superconductor. Superconductivity is extremely robust against nonmagnetic point-like disorder induced by electron irradiation. Our results place strong constraints on the previously proposed triplet pairing state by requiring fine-tuned impurity scattering amplitudes and are most naturally explained by a sign-preserving, weak-coupling, and approximately momentum-independent singlet superconducting state in $LaNiGa_2$, which does not break time-reversal symmetry. We discuss how our findings could be reconciled with previous measurements that indicated magnetic signatures in the superconducting phase.

DOI: 10.1103/PhysRevB.109.024515

I. INTRODUCTION

The centrosymmetric superconductor $LaNiGa_2$ has attracted significant attention recently [1–6], as muon spin resonance (μSR) measurements [2] reported a breaking of time-reversal symmetry in the superconducting state below $T_c \approx 2\,\mathrm{K}$. This was interpreted as nonunitary triplet superconductivity [2]. Specific heat measurements in the superconducting state suggested weak coupling *s*-wave superconductivity [1,6], also discussed theoretically [3,7], and London penetration depth measurements in polycrystalline samples indicated nodeless superconductivity [4]. These results are incompatible with a single-band time-reversal symmetry broken (TRSB) triplet state, which led to the proposal of a multiband scenario, specifically an internally antisymmetric nonunitary triplet pairing (INT) state [4,5]. For recent reviews on TRSB pairing, see Refs. [8,9]. Experimental studies of single crystals of $LaNiGa_2$ provided further support for this scenario by showing that the previously unknown Fermi surface topology of $LaNiGa_2$ possesses Dirac points at the Fermi level [6]. These Dirac points originate from the nonsymmorphic symmetry of the crystal structure (centrosymmetric, orthorhombic, space group *Cmcm* [6]), and provide the necessary band degeneracy for INT pairing [6,10]. The calculations of the electronic band structure reveal a Fermi surface with five sheets [7,10,11].

With this new information about the topologically nontrivial band structure and the availability of single crystals, it is imperative to further investigate the superconducting properties of this material. The study of single crystals is particularly important due to the significant electronic anisotropy of the superconducting state [6,10]. Also, while the possibility of a topology-enabled INT pairing is compatible with a nodeless superconducting gap with spin-triplet pairing, the effects of such a superconducting gap structure on physical properties remain to be investigated. Indeed, investigations of the multiband nature of the superconducting gap and the effects of impurity scattering require high-quality single crystals.

In this paper, we report the measurements of electrical resistivity and the variation of London penetration depth $\Delta\lambda(T) = \lambda(T) - \lambda(T_{\mathrm{min}})$, from $T_{\mathrm{min}} = 0.4\,\mathrm{K}$ to above superconducting transition temperature, $T_c \approx 2\,\mathrm{K}$. At low temperatures, $\Delta\lambda(T)$ is exponentially attenuated, confirming a fully gapped superconducting state. Although for generality we use the two-band γ model to analyze the data, the superfluid density is close to the single-gap weak-coupling *s*-wave Bardeen-Cooper-Schrieffer (BCS) [12,13] behavior. Most importantly, we used electron irradiation to introduce nonmagnetic point defects and found that the superconducting gap is robust against nonmagnetic disorder. These two independent observations point towards robust sign-preserving singlet superconductivity in $LaNiGa_2$. We discuss how these results constrain the scenarios with time-reversal symmetry breaking suggested for $LaNiGa_2$.

*Corresponding author: prozorov@ameslab.gov

II. EXPERIMENTAL METHODS

Single crystals of $LaNiGa_2$ were grown with a Ga-deficient self-flux [6]. Electrical resistivity was measured using the four-probe technique in Quantum Design PPMS. The samples were typically 1–2 mm long and had a thickness of less than 0.1 mm. For quantitative determination of electrical resistivity, contacts to the samples were made by spot welding 25-μm Au wires. These contacts are characterized by small size, resulting in high precision determination of geometric constant, and thus absolute resistivity value. The electrical resistivity at room temperature was determined as about 40 μΩ cm, based on the measurements of seven crystals. The in-plane resistivity measured along the *a* and *c* directions did not show any anisotropy within the experimental uncertainty. The *b* direction was too short to perform out-of-plane measurements. The electrical contacts for the samples used in the electron irradiation experiments were soldered with indium and mechanically reinforced with Dupont 4929 conductive silver paste [14]. These contacts were notably larger in size but were found to be stable during electron irradiation [15]. Measurements on samples with two different types of contacts were consistent within error bars of geometric factor determination.

The temperature variation of the London penetration depth, $\Delta\lambda(T) = \lambda(T) - \lambda(T_{\min})$, was measured using a sensitive frequency domain self-oscillating tunnel diode resonator (TDR) operating at a frequency of around 14 MHz. Here, $T_{\min} = 0.4$ K is set by our ^{3}He cryostat and the measurements were carried out above the superconducting transition temperature, $T_c \approx 2$ K. The low-temperature variation of $\Delta\lambda(T)$ is directly related to thermally excited quasiparticles that depend sensitively on the structure of the superconducting gap, hence the pairing state [16,17]. The experimental setup, measurements, and calibration principles are described in detail elsewhere [18,19]. For TDR measurements, the samples were cut into cuboids of typical size $0.5 \times 0.3 \times 0.04$ mm^3, where the thinnest direction corresponded to the crystallographic *b* axis. In this work precision calibration was achieved using a well-defined skin depth estimated from the measured resistivity just above T_c. The penetration depth was measured in three crystals, yielding practically identical results.

The nonmagnetic point-like disorder was introduced at the SIRIUS facility at the Laboratoire des Solides Irradiés at École Polytechnique, Palaiseau, France. Electrons accelerated to 2.5 MeV are capable of knocking out ions from their position in the crystal lattice, creating vacancy-interstitial Frenkel pairs [20–24]. To prevent recombination and clustering of freshly produced defects, irradiation was performed with a sample immersed in liquid hydrogen at about 22 K. Upon warming, some defects anneal and recombine, but due to much faster migration rates of the interstitials, a significant population of vacancies remains at room temperature. The overall effect of irradiation is characterized by electrical transport measurements that show resistivity increasing linearly with the irradiation dose. During the irradiation, the total accumulated dose of electrons propagating through the sample is measured behind the sample using a Faraday cup. The total beam current was maintained at 2.7 μA through a circular diaphragm of 5 mm in diameter, which is equivalent to the electron beam flux of 8.6×10^{13} electrons/(s cm^2). The total acquired irradiation dose is conveniently measured in C/cm^2, where 1 C/cm^2 = 6.24×10^{18} electrons/cm^2.

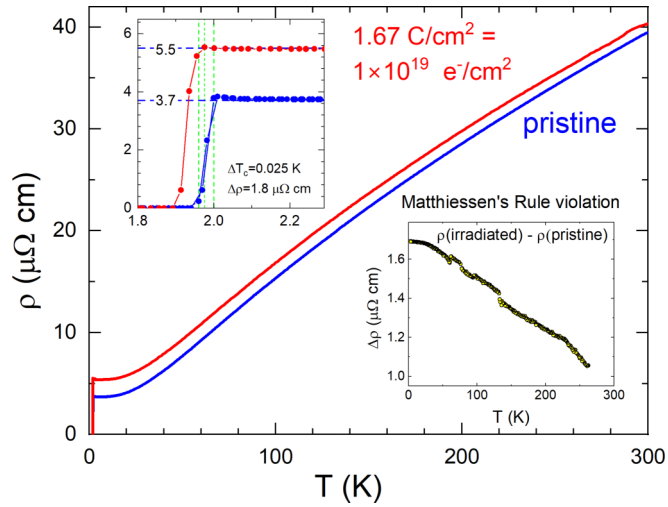

FIG. 1. Temperature-dependent resistivity of the $LaNiGa_2$ single crystal measured with current along the *c* axis before (blue curve) and after electron irradiation with a dose of 1.67 C/cm^2 (red curve). The upper inset zooms in on the superconducting transition. Irradiation has suppressed T_c by a small amount of 0.025 K (1.24%) while resulting in a significant increase of $\rho(T_c)$ from 3.7 to 5.5 μΩ cm (48.65%). The lower inset shows resistivity in a pristine state subtracted from the resistivity after the irradiation indicating some violation of the Matthiessen rule.

III. EXPERIMENTAL RESULTS

A. Electrical resistivity

The temperature-dependent resistivity of the $LaNiGa_2$ crystal in the pristine state before irradiation is shown in Fig. 1 by a blue curve. Measurements were performed with electrical current along the *c* axis on a sample with indium soldered contacts. Resistivity decreases monotonically with temperature, with a slight downward deviation from a T-linear behavior below approximately 100 K. The superconducting transition starts at $T_c \approx 2.0$ K (onset) and is reasonably sharp with the offset at $T_{c,0} \approx 1.96$ K. Electron irradiation with 1.67 C/cm^2 (red curve in Fig. 1) was performed on the same crystal to avoid uncertainty of geometric factor determination. It leads to a nearly parallel upward shift of the resistivity curve, although with some deviation from the Matthiessen rule (lower right inset) supposed to lead to a constant temperature-independent shift. Matthiessen rule violation is frequently found in materials with notable $\rho(T)$ deviations from the Bloch-Gruneisen curve [23,25,26] and is usually interpreted in multiband electronic transport models with parallel conductivity channels [25]. Upon irradiation, the superconducting transition decreased by approximately 0.025 K, which is a change of only 1.24%, while the resistivity increased by a staggering 48.65%.

B. London penetration depth

Figure 2 shows the low-temperature variation of the London penetration depth, $\Delta\lambda(T/T_c)$, with no observable change

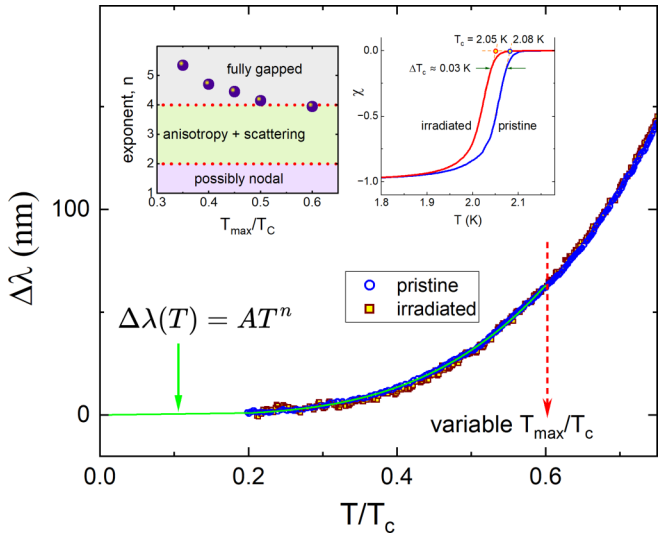

FIG. 2. Low-temperature variation of the London penetration depth $\Delta\lambda$ as a function of normalized temperature T/T_c in a pristine sample and one irradiated with a dose of 1 C/cm^2, whose data practically coincide. The solid light green line shows the best power-law fit below 0.6 T_c, with exponent $n = 3.8$. The upper right inset shows normalized magnetic susceptibility indicating a change from $T_c = 2.08$ K (pristine) to 2.05 K (irradiated). The upper left inset shows the exponent n as a function of the upper limit of the power-law fitting, $T_{\max}/T_c$.

before and after electron irradiation with the dose of 1 C/cm^2. The solid green line shows an example of a power-law fit, $\Delta\lambda(T) = A\,T^n$, in the temperature range from $T_{\min} = 0.4$ K to $T_{\max} = 1.2$ K with exponent $n = 3.8$. The fitting was repeated for several values of $T_{\max}$. The upper left inset shows the exponent n as a function of $T_{\max}/T_c$. Clearly, the fitted exponent remains above $n = 4$ up to $T_{\max} = 0.5T_c$. This type of power-law analysis has proven to be very useful when a significant variation in the temperature-dependent penetration depth was observed in iron-based superconductors [17]. It is easy to verify numerically that the exponent of $n \geqslant 4$ is practically indistinguishable from the exponential behavior. Therefore, we observed robust exponential attenuation of $\Delta\lambda(T)$ at low temperatures, suggesting a fully gapped Fermi surface in superconducting $LaNiGa_2$ crystals. This result, now obtained in single crystals, is consistent with the previous study of polycrystalline samples [4]. We also checked the change of the transition temperature upon irradiation from magnetic measurements. The upper right inset shows the temperature-dependent susceptibility of the same sample in pristine and irradiated states, focusing on T_c. Due to natural smearing, it is difficult to pinpoint T_c, but clearly only a very small downshift was induced by irradiation. This is a far cry from what is expected for a superconductor with broken time-reversal symmetry; see, for example, Ref. [27], as we analyze quantitatively in more detail below.

C. Superfluid density

The normalized superfluid density is the quantity needed for theoretical analysis. It is defined as $\rho = \lambda(0)^2/\lambda(T)^2$. Our TDR technique yields high-resolution measurements of the change of London penetration depth as a function of temperature $\Delta\lambda(T)$. However, it does not produce the absolute value $\lambda(0)$. Therefore, we use the data obtained on the crystals from the same batch that estimated the Ginzburg-Landau values of $\lambda_a^{\rm GL} = 174$ nm, $\lambda_b^{\rm GL} = 509$ nm and $\lambda_a^{\rm GL} = 189$ nm [6]. Of these, we need the penetration depth along the a and c axes. The average value in a cuboidal crystal is found from $\lambda_{ac} = (a\lambda_a + c\lambda_c)/(a + c)$ [28]. The London penetration depth at $T = 0$ is related to the Ginzburg-Landau value via $\lambda(0) = \sqrt{2}\lambda^{\rm GL}$. This follows from Eq. (25) in Ref. [17] and recalling that in the Ginzburg-Landau domain, $\lambda(T) = \lambda^{\rm GL}/\sqrt{1 - T/T_c}$. Hence, we obtain $\lambda(0) = 253$ nm. This is significantly smaller than the μSR value obtained in polycrystalline samples, $\lambda(0)_{\rm poly} = 350$ nm [2], which is expected considering the significant anisotropy of this compound. In a recent work on single crystals, in-field μSR measurements estimated $\lambda(0) = 151$ nm [29]. We will also use it for comparison. We note that these experimental values are for pristine (unirradiated) samples, but not for the theoretically clean limit, which we will denote as λ_{00} (zero scattering and zero temperature). There is always some disorder in as-grown samples.

Here, we extract the London penetration depth in the clean limit and after irradiation using a known pristine value as well as the resistivity change due to introduced disorder. This analysis is based on Tinkham's formula, which is thought to be approximate. However, we performed a direct comparison with microscopic calculations of the London penetration depth with nonmagnetic scattering using the Eilenberger approach [17] and found that it gives practically exact agreement at least for an isotropic Fermi surface and s-wave pairing. According to Tinkham [30],

$$\lambda(\Gamma) = \lambda_{00}\sqrt{1 + \frac{\xi_0}{\ell}}, \tag{1}$$

where ℓ is electronic mean free path and $\xi_0 = \hbar v/\pi\Delta_0$ is the BCS [12,13] coherence length, not to be confused with the coherence length determined by the upper critical field, $\xi^2 = \phi_0/2\pi H_{c2}$, where ϕ_0 is the magnetic flux quantum, v is Fermi velocity, and Δ_0 is the superconducting gap at zero temperature. The clean limit λ_{00} does not depend on any superconducting parameters and is given by the London theory,

$$\lambda_{00}^2 = \frac{m}{\mu_0 n e^2}, \tag{2}$$

where m and e are electron mass and charge, respectively, and n is electron concentration. At the same simple isotropic level, the Drude resistivity is

$$\rho = \frac{mv}{ne^2\ell}, \tag{3}$$

and so we can write

$$\frac{\rho}{\lambda_{00}^2} = \frac{\mu_0 v}{\ell} = \frac{\mu_0}{\tau}, \tag{4}$$

where $\tau = \ell/v$ is the scattering time. Therefore, the mean free path is given by

$$\ell = \frac{\mu_0 v \lambda_{00}^2}{\rho}. \tag{5}$$

We can now evaluate λ_{00} using Eq. (1), where we substitute Eq. (5) to trivially obtain

$$\lambda_{00}^2 = \lambda(\Gamma)^2 - \frac{\rho\xi_0}{\mu_0 v}. \tag{6}$$

Now we can use the measured resistivity after irradiation to estimate the change in the London penetration depth. This procedure also gives a way to estimate the current state (clean or dirty) of any sample, irradiated or pristine.

We use literature data for the Fermi velocity, $v = 3 \times 10^5$ m/s [11], Debye temperature, $T_D = 166$ K [6], and the value of London penetration depth determined by the μSR measurements, $\lambda_{pr} = 253$ nm [6]. With $T_c = 2.0$ K, we estimate the zero-temperature superconducting gap using a standard BCS ratio, $\Delta_0 = 1.7638 k_B T_c \approx 0.3$ meV [12,13]. Therefore, the BCS coherence length is $\xi_0 = \hbar v/\pi\Delta_0 = 207$ nm.

As can be seen in Fig. 1, the resistivity changed from 3.7 μΩ cm to 5.5 μΩ cm upon 2.5-MeV electron irradiation with the total fluence of 1.67 C/cm^2 $= 1 \times 10^{19}$ e$^-$/cm^2. First, we estimate the clean-limit penetration depth from Eq. (6), $\lambda_{00} = 209$ nm for the case when a magnetic field is applied along the b axis. With this value, we can now extract the London penetration depth after the irradiation. Using Eq. (5), the mean free path before irradiation is $\ell_{\text{pristine}} = 445$ nm, and after it is $\ell = 300$ nm. Therefore, using Eq. (1), we obtain $\lambda_{\text{irr}} = 282$ nm. Note that the criterion distinguishing between clean and dirty limit is based on the dimensionless scattering rate, $\Gamma = \hbar v/2\pi T_c \ell \approx 0.882\xi_0/\ell$. The latter is simply obtained from the above equations and was obtained long ago by Helfand and Wetzmeier [32]. This shows the importance of the BCS coherence length as the relevant scale for scattering. In the present case, we start at $\Gamma_{\text{pristine}} \approx 0.41$ and after irradiation, we obtain $\Gamma \approx 0.61$. From the analysis we obtain that the scattering rate changes with the dose of electron irradiation as $d\Gamma/d(\text{dose}) \approx 0.12$, where the dose is measured in C/cm^2. One might wonder whether this background amount of disorder in the pristine sample could already be sufficient to drive the system from the TRSB state into a state with time-reversal symmetry (TRS), since disorder suppresses T_c of the TRSB triplet state much faster than T_c of a (possibly competing) TRS-preserving singlet state. However, since the difference between the $T_c = 2.1$ K (onset) reported in Ref. [2] for the TRSB and our observed $T_c = 1.96$ K before irradiation is so small (only 0.14 K or about 6.7% of T_c), this would require a large degree of fine tuning to have a singlet and triplet energetically close to each other. We discuss this further in Sec. IV.

Although this is not an ultraclean limit, it is moderately clean (as long as $\Gamma < 1$). This is important because now we can use the two-band γ model, so far developed only in the clean limit [31] to fit the superfluid density. It is constructed from the measured change of the penetration depth, $\Delta\lambda(T)$, shown in Fig. 2,

$$\rho_s(T) = \left(\frac{\lambda(0)}{\lambda(T)}\right)^2 = \left(1 + \frac{\Delta\lambda(T)}{\lambda(0)}\right)^{-2}. \tag{7}$$

Here, we used the fact that at low temperatures $\Delta\lambda(T)$ is exponentially attenuated, see Fig. 2, so we can assume with good accuracy that $\Delta\lambda(T) \equiv \lambda(T) - \lambda(T_{\text{min}}) \approx \lambda(T) - \lambda(0)$.

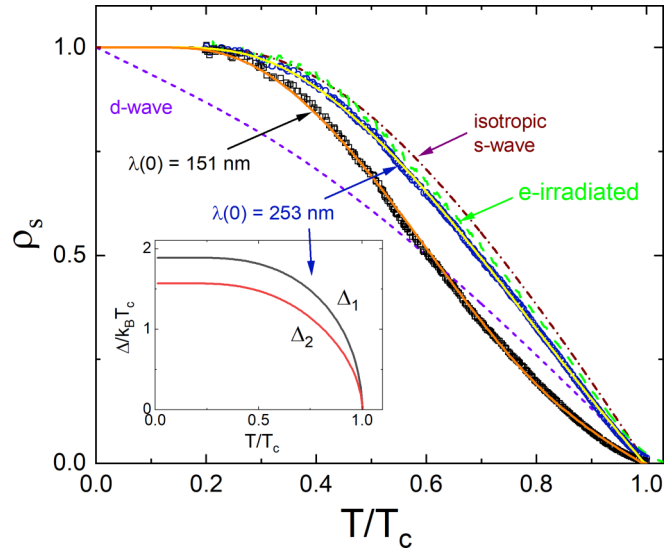

FIG. 3. Superfluid density obtained from the London penetration depth shown in Fig. 2 using experimental (μSR) $\lambda(0) = 253$ nm [6] for the pristine sample (blue circles) and $\lambda(0) = 282$ nm for the irradiated sample (green dashed line), obtained as described in the text. The yellow line shows an excellent γ-model [31] fit of the data. Standard d- and s-wave curves are shown by dashed and dash-dotted lines, respectively. Inset shows two superconducting gaps obtained self-consistently from the fit. For comparison, the superfluid density obtained using $\lambda(0) = 151$ nm [29] along with a γ-model fit are also shown by the black squares and an orange solid curve, respectively.

Figure 3 shows the superfluid density before (blue circles) and after (dashed green line) electron irradiation using Eq. (7) with the experimental (μSR) $\lambda(0) = \lambda_{pr} = 253$ nm [6] for the pristine sample and $\lambda(0) = \lambda_{\text{irr}} = 282$ nm for the irradiated sample, estimated as described above. For comparison, the superfluid density obtained using $\lambda(0) = 151$ nm [29] along with a γ-model fit are also shown by the black squares and an orange solid curve, respectively. The yellow line shows an excellent γ-model [31] fit of the data for the pristine sample. The superfluid density of the irradiated sample is shifted to slightly higher values, consistent with the increased $\lambda(0)$. Considering the close proximity of the two curves, there was no reason to fit the irradiated sample. The standard d- and s-wave curves are shown by dashed and dash-dotted lines, respectively. The inset shows two superconducting gaps obtained self-consistently from the fit.

D. Self-consistent γ-model fitting

Assuming isotropic superconducting order parameters, the γ model takes as input the average Fermi velocities and the densities of states (DOS) on the effective bands as well as the interaction matrix $\lambda_{i,j}$ [17,31]. Here, we consider all of these values as free fitting parameters. Note that $\lambda_{i,j}$ should not be confused with the penetration depth λ. The third interaction parameter is constrained by the value of T_c calculated from the effective interaction constant λ_{eff} as $1.7638 k_B T_c = 2\hbar\omega_D \exp(-\lambda_{\text{eff}}^{-1})$. Here, the effective interaction constant λ_{eff} is obtained from the solution of algebraic equations containing all the coefficients $\lambda_{i,j}$; see Sec. II A of Ref. [31],

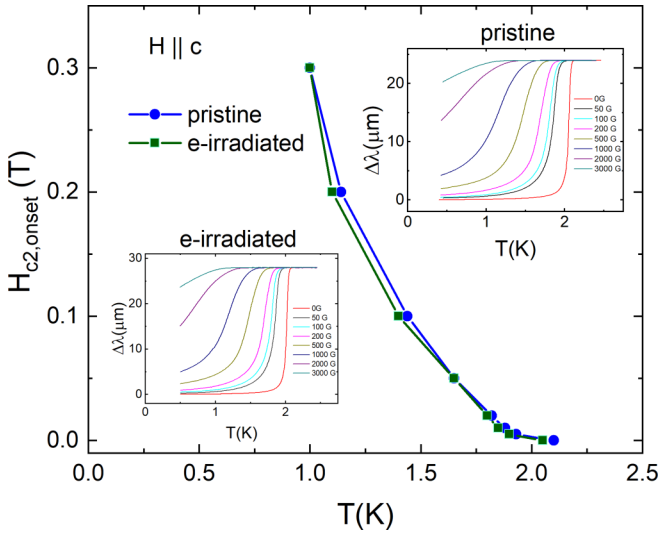

FIG. 4. Upper critical field H_{c2} measured in pristine and irradiated samples obtained from the onset of a diamagnetic signal in the TDR $\Delta\lambda(T)$ curves shown in the upper-right and bottom-left insets, respectively.

and Debye temperature, $T_D = 166\,\mathrm{K}$ [6], assuming phonon-mediated superconductivity. For a different "glue," there will be a different similar quantity. The fitting is performed in MATLAB by solving self-consistency equations for two order parameters at each temperature, $t = T/T_c$, then calculating the partial superfluid densities, $\rho_1(t)$ and $\rho_2(t)$, and finally performing nonlinear optimization comparing experimental points with the calculated total superfluid density, $\rho(t) = \gamma\rho_1(t) + (1-\gamma)\rho_2(t)$. With $T_c = 2.0\,\mathrm{K}$ and a fixed $n_1 = 0.5$, we obtained from the fit of the pristine data, $\lambda_{11} = 0.416$, $\lambda_{22} = 0.388$, $\lambda_{12} = 0.036$, $\gamma = 0.300$ and the effective $\lambda_{\mathrm{eff}} = 0.220$. Therefore, we have two fairly similar, at first sight, barely coupled bands, which is probably why they do not form a single gap everywhere. The key to the γ model is $\gamma = n_1 v_1^2/(n_1 v_1^2 + n_2 v_2^2)$, where v_i are the Fermi velocities on different bands. From the fit we see that $v_1 < v_2$, which may mean that the carriers on band 1 are heavier. As such, they will contribute the most to the specific heat that appears as if there were a single band [6]. The opposite is true for superfluid density, where light carriers contribute the most. We note, however, that the specific heat calculated with the above parameters is already quite close to the experiment considering that the superfluid density is quite close to the single-band s-wave BCS curve. Fitting the superfluid density calculated with $\lambda(0) = 151\,\mathrm{nm}$, we obtained $\lambda_{11} = 0.440$, $\lambda_{22} = 0.401$, $\lambda_{12} = 0.012$, $\gamma = 0.300$ and the effective $\lambda_{\mathrm{eff}} = 0.222$, which does not alter the above conclusions in any way, only showing even weaker interband coupling.

E. Upper critical field

Finally, we discuss the upper critical field H_{c2} displayed in Fig. 4. The $H_{c2}(T)$ was estimated from the onset of a diamagnetic signal in the TDR $\Delta\lambda(T)$ curves shown in the upper right and lower left insets, respectively. While all other properties show quite conventional behavior, $H_{c2}(T)$ exhibits an unusual convex shape. However, we note that the TDR curves not only shift, but also broaden significantly, making it difficult to extract the precise H_{c2} values. A similar behavior, convex curvature and broadening, was previously observed in AC susceptibility measurements in polycrystalline samples [4].

Curiously, there is practically no change in $H_{c2}(T)$ after electron irradiation. However, both this observation and the convex curvature can be easily understood within multiband superconductivity [33–35], confirming what we already learned from the analysis of the superfluid density. Importantly, the upper critical field is small. If triplet pairing was present, one would expect a large upper critical field, like in UTe_2. On the other hand, $LaNiGa_2$ is not a heavy fermion material, so it would be subject to a smaller orbital limit [6].

IV. DISCUSSION

We now discuss the relation of our findings to the pairing states of previous works [2,4]. The fact that our penetration depth data can be fitted with a fully gapped order parameter that has two different magnitudes on two different (subsets of) bands in the system is consistent with previous works: in previous experiments on polycrystalline samples, the two gap values were $\Delta_1(0)/k_BT_c = 2.04$ and $\Delta_2(0)/k_BT_c = 1.29$ [4]; meanwhile we obtained closer ratios of 1.89 and 1.57, respectively. The difference is most likely due to a significant anisotropy of the penetration depth. While having several rather than one single gap magnitude is, in fact, the expected behavior for a complex multiband superconductor, previous μSR measurements in $LaNiGa_2$ [2] have indicated broken time-reversal symmetry in its superconducting state—a far less common phenomenon. In that context, our measurements of the effects of irradiation provide particularly strong constraints, which we discuss next.

As illustrated in Fig. 5(a), showing the suppression of the critical temperature of $LaNiGa_2$ along with that of unconventional superconductors and the Abrikosov-Gorkov (AG) curve for magnetic scattering in a BCS state, the suppression of T_c with disorder is very weak. More quantitatively, we extract a value of the dimensionless sensitivity to disorder scattering ζ [15] given by

$$\zeta = 2\pi^{-2}[d(\Delta T_c/T_{c0})/d\Gamma] \approx 0.0124. \tag{8}$$

To demonstrate that this is difficult to reconcile with time-reversal symmetry breaking in the superconducting state, we next focus on the most favorable scenario of an order parameter that does not depend on momentum. Due to the low point group (D_{2h}) symmetries of $LaNiGa_2$, nonunitary triplet pairing has been argued to be the most natural realization of broken time-reversal symmetry [2]. Since a triplet superconducting order parameter is symmetric in spin space, the absence of nodes necessitates involving more than one orbital degree of freedom [4,5] to make the entire order parameter antisymmetric; the simplest limit of such an INT state involves only two orbitals (Pauli matrices σ_j), reading as $\Delta = \boldsymbol{d}\cdot\boldsymbol{s}\,i\sigma_y$, where $\boldsymbol{s} = (s_x, s_y, s_z)$ are the spin Pauli matrices and $\boldsymbol{d}$ is the triplet vector. Although only $\boldsymbol{d}$ with $\boldsymbol{d}^* \times \boldsymbol{d} \neq 0$ is consistent with the broken time-reversal symmetry, we will not further specify $\boldsymbol{d}$ as the following statements do not depend on the specific form of $\boldsymbol{d}$.

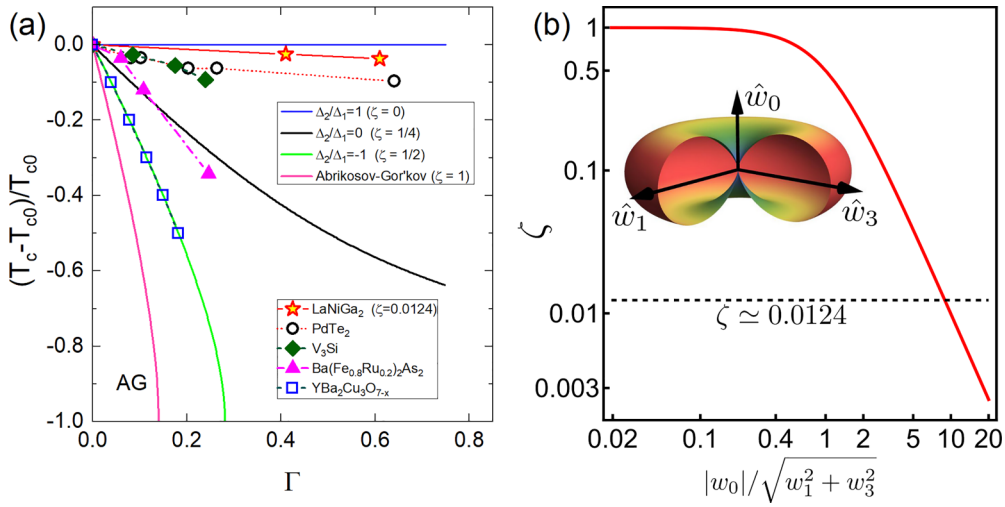

FIG. 5. (a) Comparison of the disorder sensitivity of the transition temperature in $LaNiGa_2$ with other superconductors (symbols). The solid lines show the expectations for two isotropic gaps with different gap ratios. The corresponding parameter ζ is shown. (b) Dimensionless disorder-sensitivity parameter ζ, see Eq. (9), shown as a function of $\hat{w}_j = w_j/|\boldsymbol{w}|$ (inset shows spherical plot with radius proportional to ζ) and $|w_0|/\sqrt{w_1^2+w_3^2}$ (main panel, red), and extracted from the measurements of irradiated samples (dashed, main panel).

To model disorder for electron-irradiation experiments, we make the common assumption of nonmagnetic and spin-rotation-invariant impurities that are point-like, i.e., scatter between all momenta within the Brillouin zone with equal amplitude; the associated scattering matrix (a 4×4 matrix in spin and orbital space) can then be parametrized as $W = s_0 \otimes (w_0\sigma_0 + w_1\sigma_x + w_3\sigma_z)$, where $w_j \in \mathbb{R}$. Intuitively, $w_0 \pm w_3$ captures the amplitude of the scattering within each of the two bands ($\pm$) while w_1 describes the interband scattering. Further, making the most favorable assumption for superconductivity that the two bands are approximately degenerate (on the scale of Δ), which in fact is imposed by the nonsymmorphic symmetry [10], we can readily apply the generalized Anderson theorem of [15] and find

$$\zeta = \frac{w_1^2 + w_3^2}{w_0^2 + w_1^2 + w_3^2}. \tag{9}$$

We can see that both interband (w_1) scattering as well as a scattering imbalance (w_3) between the two bands are pair breaking. It might hold that $w_3 \ll w_0$, but it seems less plausible that $w_1 \ll w_0$. In fact, as also illustrated visually in Fig. 5(b), the obtained $\zeta \approx 0.0124$ gives a very strong constraint on the matrix elements—quantitatively, we find $|w_0|/\sqrt{w_1^2+w_3^2} = \sqrt{\zeta^{-1}-1} \simeq 8.9$. We note that generalizing to momentum-dependent superconducting order parameters would make the pairing state further susceptible to w_0, as one can immediately conclude from the generalized Anderson theorem [15]. As such, it would even increase its sensitivity and does not help with reconciling broken time-reversal symmetry and our irradiation data.

One alternative possibility is that the time-reversal symmetry breaking superconducting state is the leading instability only by a small margin and there is an almost degenerate subleading state in the spin singlet channel [recall that Eq. (9) holds for $\Delta = \boldsymbol{d}\cdot\boldsymbol{s}\, i\sigma_y$ irrespective of the form of $\boldsymbol{d}$]. Then, either our "pristine" sample already exhibits enough disorder to favor that subleading singlet state or only the amount of disorder resulting from irradiation did. Note that this subleading singlet state must preserve time-reversal symmetry since the point group D_{2h} of the system only admits one-dimensional irreducible representations. Taking the critical temperatures $T_c \approx 2.1\,\mathrm{K}$ (onset), $1.96\,\mathrm{K}$, and $1.94\,\mathrm{K}$ from Ref. [2], our pristine sample, and our irradiated sample, respectively, we conclude that this degeneracy must be within at most $0.16\,\mathrm{K}$, i.e., about only 8% of T_c. Therefore, also this scenario requires some fine-tuning assumption, similar to the constraint on the disorder matrix elements, $|w_0|/\sqrt{w_1^2+w_3^2} \approx 8.9$, noted above.

Finally, the third possibility is that the perfectly homogeneous system prefers a time-reversal preserving spin-singlet state (consistent with our irradiation study) which, due to a subleading triplet or singlet superconducting instability, exhibits time-reversal symmetry breaking *local* patterns around impurities [36,37]. These could be picked up by local probes like μSR. To exclude or confirm this scenario, further irradiation studies in combination with μSR would be required.

V. CONCLUSIONS

To summarize the experimental findings, thermodynamic and transport measurements in high-quality $LaNiGa_2$ crystals are quantitatively consistent with a non-sign-changing multigap superconducting state with almost equal but barely coupled bands, one heavier and another lighter. The most striking observation is that superconductivity is extremely robust to disorder and the transition temperature did not change significantly after electron irradiation; meanwhile, the resistivity changed by about 50%, indicating that the irradiation indeed produced nonmagnetic scattering centers. More quantitatively, we find a disorder sensitivity parameter $\zeta \approx 0.0124$, much smaller than the value $1/2$ for a (single-band) superconducting order parameter transforming under a nontrivial irreducible representation [15]. Being sensitive to the relative

phase of the superconducting order parameter on different parts of the Fermi surface, the remarkably weak disorder sensitivity yields very strong constraints on superconductivity: we find that the INT state [4,5] is only consistent with this observation if pair-breaking scattering due to interband transitions and a scattering imbalance between the bands is about nine times weaker than non-pair-breaking scattering. This implies that intraband matrix elements of the impurities must be at least nine times larger than the interband contributions—a rather unwonted scenario. Therefore, we identified and discussed two alternative possibilities to reconcile these findings with previous μSR measurements, finding a time-reversal symmetry breaking state [2]. The first scenario is based on the assumption that the nonunitary INT superconductor is indeed the leading instability but very closely followed by a time-reversal symmetric singlet phase that is favored by the disorder we introduce. Our estimates, however, reveal that this requires a similar amount of fine-tuning as the aforementioned scenario, involving the impurity matrix elements. In the second alternative scenario the homogeneous bulk superconducting phase is a time-reversal symmetry preserving singlet state while the moments picked up by μSR are related to disorder-induced local fields associated with the admixture of a competing superconducting state with nontrivial complex phases [36,37]. Our findings reveal that the microscopic form of the superconducting state in $LaNiGa_2$ is still an open question and call for further experimental and theoretical work to pinpoint which scenario is realized.

Note added. Just before posting our article, another work appeared [38] in which nuclear magnetic resonance (NMR) measurements of $LaNiGa_2$ crystals found no enhancement of paramagnetism or magnetic fluctuations and yielded a Korringa ratio different from that of other time-reversal symmetry breaking superconductors. These observations are in agreement with our conclusions.

ACKNOWLEDGMENTS

This work was supported by the U.S. Department of Energy (DOE), Office of Science, Basic Energy Sciences, Materials Science and Engineering Division. Ames Laboratory is operated for the U.S. DOE by Iowa State University under Contract No. DE-AC02-07CH11358. Electron irradiation was supported by "Investissements d'Avenir" LabEx PALM (ANR-10-LABX-0039-PALM). The authors acknowledge support from the EMIR&A French network (FR CNRS 3618) on the platform SIRIUS at Ecole Polytechnique in Palaiseau, France. Sample synthesis at UC Davis was supported by the UC Laboratory Fees Research Program (LFR-20-653926). M.S.S. acknowledges funding by the European Union (ERC-2021-STG, Project 101040651—SuperCorr). Views and opinions expressed are, however, those of the authors only and do not necessarily reflect those of the European Union or the European Research Council Executive Agency. Neither the European Union nor the granting authority can be held responsible for them.

[1] N. L. Zeng and W. H. Lee, Superconductivity in the Ni-based ternary compound $LaNiGa_2$, Phys. Rev. B **66**, 092503 (2002).
[2] A. D. Hillier, J. Quintanilla, B. Mazidian, J. F. Annett, and R. Cywinski, Nonunitary triplet pairing in the centrosymmetric superconductor $LaNiGa_2$, Phys. Rev. Lett. **109**, 097001 (2012).
[3] H. M. Tütüncü and G. P. Srivastava, Origin of superconductivity in layered centrosymmetric $LaNiGa_2$, Appl. Phys. Lett. **104**, 022603 (2014).
[4] Z. F. Weng, J. L. Zhang, M. Smidman, T. Shang, J. Quintanilla, J. F. Annett, M. Nicklas, G. M. Pang, L. Jiao, W. B. Jiang, Y. Chen, F. Steglich, and H. Q. Yuan, Two-gap superconductivity in $LaNiGa_2$ with nonunitary triplet pairing and even parity gap symmetry, Phys. Rev. Lett. **117**, 027001 (2016).
[5] S. K. Ghosh, G. Csire, P. Whittlesea, J. F. Annett, M. Gradhand, B. Újfalussy, and J. Quintanilla, Quantitative theory of triplet pairing in the unconventional superconductor $LaNiGa_2$, Phys. Rev. B **101**, 100506(R) (2020).
[6] J. R. Badger, Y. Quan, M. C. Staab, S. Sumita, A. Rossi, K. P. Devlin, K. Neubauer, D. S. Shulman, J. C. Fettinger, P. Klavins *et al.*, Dirac lines and loop at the Fermi level in the time-reversal symmetry breaking superconductor $LaNiGa_2$, Commun. Phys. **5**, 22 (2022).
[7] D. J. Singh, Electronic structure and fermiology of superconducting $LaNiGa_2$, Phys. Rev. B **86**, 174507 (2012).
[8] S. K. Ghosh, M. Smidman, T. Shang, J. F. Annett, A. D. Hillier, J. Quintanilla, and H. Yuan, Recent progress on superconductors with time-reversal symmetry breaking, J. Phys.: Condens. Matter **33**, 033001 (2021).
[9] A. Ramires, Nonunitary superconductivity in complex quantum materials, J. Phys.: Condens. Matter **34**, 304001 (2022).
[10] Y. Quan, V. Taufour, and W. E. Pickett, Nonsymmorphic band sticking in a topological superconductor, Phys. Rev. B **105**, 064517 (2022).
[11] I. Hase and T. Yanagisawa, Electronic structure of $LaNiGa_2$, J. Phys. Soc. Jpn. **81**, 103704 (2012).
[12] J. Bardeen, L. N. Cooper, and J. R. Schrieffer, Microscopic theory of superconductivity, Phys. Rev. **106**, 162 (1957).
[13] J. Bardeen, L. N. Cooper, and J. R. Schrieffer, Theory of superconductivity, Phys. Rev. **108**, 1175 (1957).
[14] M. A. Tanatar, A. E. Böhmer, E. I. Timmons, M. Schütt, G. Drachuck, V. Taufour, K. Kothapalli, A. Kreyssig, S. L. Bud'ko, P. C. Canfield, R. M. Fernandes, and R. Prozorov, Origin of the resistivity anisotropy in the nematic phase of FeSe, Phys. Rev. Lett. **117**, 127001 (2016).
[15] E. I. Timmons, S. Teknowijoyo, M. Kończykowski, O. Cavani, M. A. Tanatar, S. Ghimire, K. Cho, Y. Lee, L. Ke, N. H. Jo, S. L. Bud'ko, P. C. Canfield, P. P. Orth, M. S. Scheurer, and R. Prozorov, Electron irradiation effects on superconductivity in $PdTe_2$: An application of a generalized Anderson theorem, Phys. Rev. Res. **2**, 023140 (2020).
[16] R. Prozorov and R. W. Giannetta, Magnetic penetration depth in unconventional superconductors, Supercond. Sci. Technol. **19**, R41 (2006).
[17] R. Prozorov and V. G. Kogan, London penetration depth in iron-based superconductors, Rep. Prog. Phys. **74**, 124505 (2011).

[18] R. Prozorov, R. W. Giannetta, A. Carrington, P. Fournier, R. L. Greene, P. Guptasarma, D. G. Hinks, and A. R. Banks, Measurements of the absolute value of the penetration depth in high-T_c superconductors using a low-T_c superconductive coating, Appl. Phys. Lett. **77**, 4202 (2000).

[19] R. Prozorov, Meissner-London susceptibility of superconducting right circular cylinders in an axial magnetic field, Phys. Rev. Appl. **16**, 024014 (2021).

[20] A. C. Damask and G. J. Dienes, *Point Defects in Metals* (Gordon & Breach Science Publishers, 1963).

[21] M. W. Thompson, *Defects and Radiation Damage in Metals* (Cambridge University Press, Cambridge, 1974).

[22] R. Prozorov, M. Kończykowski, M. A. Tanatar, A. Thaler, S. L. Bud'ko, P. C. Canfield, V. Mishra, and P. J. Hirschfeld, Effect of electron irradiation on superconductivity in single crystals of $Ba(Fe_{1-x}Ru_x)_2As_2 (x = 0.24)$, Phys. Rev. X **4**, 041032 (2014).

[23] K. Cho, M. Kończykowski, S. Teknowijoyo, M. A. Tanatar, and R. Prozorov, Using electron irradiation to probe iron-based superconductors, Supercond. Sci. Technol. **31**, 064002 (2018).

[24] K. Cho, M. Kończykowski, S. Teknowijoyo, M. A. Tanatar, J. Guss, P. B. Gartin, J. M. Wilde, A. Kreyssig, R. J. McQueeney, A. I. Goldman, V. Mishra, P. J. Hirschfeld, and R. Prozorov, Using controlled disorder to probe the interplay between charge order and superconductivity in $NbSe_2$, Nat. Commun. **9**, 2796 (2018).

[25] J. Bass, Deviations from Matthiessen's rule, Adv. Phys. **21**, 431 (1972).

[26] R. Prozorov, M. Kończykowski, M. A. Tanatar, H.-H. Wen, R. M. Fernandes, and P. C. Canfield, Interplay between superconductivity and itinerant magnetism in underdoped $Ba_{1-x}K_xFe_2As_2$ ($x = 0.2$) probed by the response to controlled point-like disorder, npj Quantum Mater. **4**, 34 (2019).

[27] S. Ghimire, M. Kończykowski, K. Cho, M. A. Tanatar, D. Torsello, I. S. Veshchunov, T. Tamegai, G. Ghigo, and R. Prozorov, Effect of controlled artificial disorder on the magnetic properties of $EuFe_2(As_{1-x}P_x)_2$ ferromagnetic superconductor, Materials (MDPI) **14**, 3267 (2021).

[28] R. Prozorov, Linear magnetic susceptibility of anisotropic superconductors of cuboidal shape, J. Appl. Phys. **134**, 063901 (2023).

[29] S. Sundar, M. Yakovlev, N. Azari, M. Abedi, D. M. Broun, H. U. Ozdemir, S. R. Dunsiger, D. Zackaria, V. Taufour, and J. E. Sonier, Gap structure of the non-symmorphic superconductor $LaNiGa_2$ probed by muSR, arXiv:2311.00069 (2023).

[30] M. Tinkham, *Introduction to Superconductivity* (Courier Corporation, Boston, 2004).

[31] V. G. Kogan, C. Martin, and R. Prozorov, Superfluid density and specific heat within a self-consistent scheme for a two-band superconductor, Phys. Rev. B **80**, 014507 (2009).

[32] E. Helfand and N. R. Werthamer, Temperature and purity dependence of the superconducting critical field, H_{c2}. II, Phys. Rev. **147**, 288 (1966).

[33] H. Suderow, V. G. Tissen, J. P. Brison, J. L. Martínez, S. Vieira, P. Lejay, S. Lee, and S. Tajima, Pressure dependence of the upper critical field of MgB_2 and of YNi_2B_2C, Phys. Rev. B **70**, 134518 (2004).

[34] S. V. Shulga, S.-L. Drechsler, G. Fuchs, K.-H. Müller, K. Winzer, M. Heinecke, and K. Krug, Upper critical field peculiarities of superconducting YNi_2B_2C and $LuNi_2B_2C$, Phys. Rev. Lett. **80**, 1730 (1998).

[35] H. Suderow, V. G. Tissen, J. P. Brison, J. L. Martínez, and S. Vieira, Pressure induced effects on the Fermi surface of superconducting $NbSe_2$, Phys. Rev. Lett. **95**, 117006 (2005).

[36] Z.-X. Li, S. A. Kivelson, and D.-H. Lee, Superconductor-to-metal transition in overdoped cuprates, npj Quantum Mater. **6**, 36 (2021).

[37] C. N. Breiø, P. J. Hirschfeld, and B. M. Andersen, Supercurrents and spontaneous time-reversal symmetry breaking by nonmagnetic disorder in unconventional superconductors, Phys. Rev. B **105**, 014504 (2022).

[38] P. Sherpa, I. Vinograd, Y. Shi, S. A. Sreedhar, C. Chaffey, T. Kissikov, M. C. Jung, A. S. Bontana, A. P. Dioguardi, R. Yamamoto, M. Hirata, G. Conti, S. Nemsak, J. R. Badger, P. Klavins, I. Vishik, V. Taufour, and N. J. Curro, Absence of strong magnetic fluctuations or interactions in the normal state of $LaNiGa_2$, arXiv:2311.06988 (2023).